Journal of Macromolecular Science, Part A
Publication details, including instructions for authors and subscription information:
http://www.informaworld.com/smpp/title~content=t713597274

Characterization of Phase Behavior in Polymer Blends by Light Scattering

Takashi Inoue[a]; Toshiaki Ougizawa[ab]
[a] Department of Organic and Polymeric Materials, Tokyo Institute of Technology Ookayama, Tokyo, Japan [b] Central Research and Development Department, Experimental Station. E. I. du Pont de Nemours & Company, Wilmington, Delaware

To cite this Article Inoue, Takashi and Ougizawa, Toshiaki(1989) 'Characterization of Phase Behavior in Polymer Blends by Light Scattering', Journal of Macromolecular Science, Part A, 26: 1, 147 — 173
To link to this Article: DOI: 10.1080/00222338908053847
URL: http://dx.doi.org/10.1080/00222338908053847

J. MACROMOL. SCI.–CHEM., A26(1), pp. 147-173 (1989)

CHARACTERIZATION OF PHASE BEHAVIOR IN POLYMER BLENDS BY LIGHT SCATTERING

TAKASHI INOUE* and TOSHIAKI OUGIZAWA†

Department of Organic and Polymeric Materials
Tokyo Institute of Technology
Ookayama, Meguro-ku, Tokyo 152, Japan

1. INTRODUCTION

It is well known that most pairs of high molecular weight polymers are immiscible. This is so because the combinatorial entropy of mixing of two polymers is dramatically less than that of two low molecular weight compounds [1-3]. The enthalpy of mixing, on the other hand, is often a positive quantity. Therefore, dissimilar polymers are only miscible if there are favorable specific interactions between them leading to a negative contribution to the Gibbs free energy of mixing. Miscible polymers tend to phase separate at elevated temperatures. This lower critical solution temperature (LCST) behavior is interpreted in terms of the equation of state or the free-volume contribution [1-3]. About 30 pairs of dissimilar polymers have been found to exhibit the LCST behavior.

The LCST behavior provides a new prospect for the design of supermolecular structure in polymer blends. For instance, if a homogeneous mixture of dissimilar polymers is allowed to undergo a rapid temperature jump from below LCST to above LCST, spinodal decomposition takes place and a highly interconnected two-phase morphology with uniform domain size (so-called "modulated structure") develops. Of course, by quenching the phase-sepa-

*To whom correspondence should be addressed.
†Present address: Central Research and Development Department, Experimental Station. E. I. du Pont de Nemours & Company, Wilmington, Delaware 19898.

rated system below the glass transition temperature after an appropriate time of phase separation, we are able to fix or freeze this characteristic morphology.

Unfortunately, the formation of modulated structure by thermally induced phase separation is limited to binary polymer systems having a LCST phase diagram. If we use a common solvent for both polymers, we are able to prepare a polymer blend with modulated structure by solution casting, even for combinations of immiscible polymers [4]. This implies that the potential for the design of polymer blends with modulated structure is expanded to a much wider variety of combinations of dissimilar polymers. Actually, some fine materials have been exploited by the solution casting of dissimilar polymers, e.g., a charge-mosaic membrane [5], an artificial paper for digital full-color heat-set printing [6], and highly deformable plastics [7].

For such design of new materials by polymer blending, one needs a basic understanding of phase behavior: phase equilibrium, kinetics of phase separation, and kinetics of phase dissolution, in binary polymer-polymer systems and also ternary polymer systems consisting of two dissimilar polymers and a solvent. In this article we deal with such subjects mostly by using various light-scattering methods.

First, in Section 2 we briefly describe the formation of modulated structures by solution casting of polymer blends. This corresponds to the preparation of novel specimens for light-scattering studies. In other words, a combination of the novel specimen and light-scattering technique yields a simple and elegant procedure to estimate the phase diagram and the kinetics of phase dissolution, as will be discussed in Section 3. Section 4 is devoted to a kinetic study of phase decomposition of ternary polymer solutions. From the analysis of the kinetic variables, we show how to determine the phase diagram in terms of the spinodal curve. In Section 5 we indicate another light-scattering method based on the de Gennes' scattering function in the single-phase region. For this scattering method we introduce a modified version of the scattering function for ternary polymer solutions and estimate the correlation length. From both the temperature and the concentration dependence of the correlation length, we also characterize the phase behavior.

2. POLYMER BLENDS WITH MODULATED STRUCTURE

Generally speaking, solution casting of immiscible polymer blends results in two-phase morphology with irregular shape and size of domain. A typical example is shown in Fig. 1(a). It is a light micrograph of a 50/50 blend of

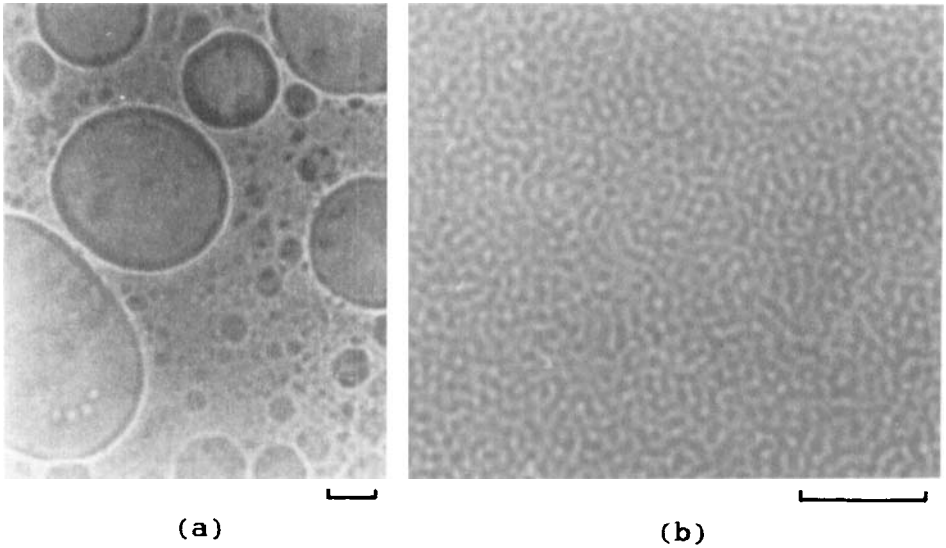

FIG. 1. Light micrographs of solution-cast films of polymer blends. (a) 50/50 Polystyrene/BR. (b) 50/50 BR/SBR-45. Scale bar: 10 μm. BR is a *cis*-1,4-polybutadiene prepared by solution polymerization with Ti catalyst (JSR BR02; $M_w = 39 \times 10^4$, $M_n = 18 \times 10^4$). SBR-45 is a poly(styrene-*co*-butadiene) containing 45 wt% styrene prepared by emulsion polymerization (JSR SBR0202; $M_w = 48 \times 10^4$, $M_n \times 10^4$).

polystyrene/polybutadiene cast from toluene solution at a few wt% of total polymer in which there are isolated spherical domains with diameters ranging from a few μm to about 50 μm. In contrast to the irregular two-phase morphology, we found a regular morphology in solution-cast films of immiscible polymers [4], as is typically shown in Fig. 1(b). In this light micrograph of a 50/50 blend of BR/SBR-45, characteristic features of the morphology are regular, with a periodic distance of about 1.5 μm, and dual connectivity of phases.

The morphology is quite similar in appearance to the two-dimensional representation of the phase structure simulated by Cahn [9], according to his linear theory of spinodal decomposition. It is shown that, in fact, the regular structure in Fig. 1(b) develops by spinodal decomposition during solution casting of the ternary polymer solution. Hereafter, the structure will be referred to as a "modulated structure," as has been done in the fields

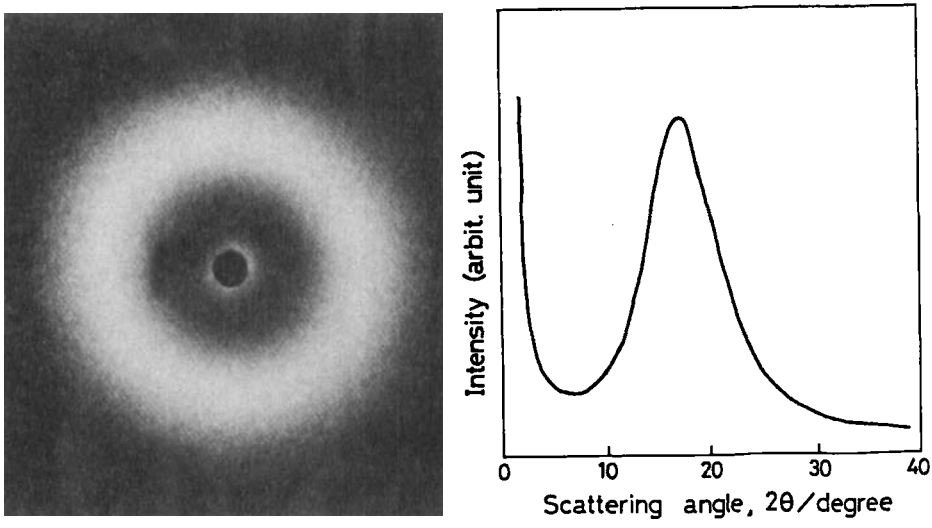

FIG. 2. (a) Light-scattering pattern (V_v) from the BR/SBR-45 blend film of Fig. 1(a) by the photographic technique (12), and (b) its goniometer trace obtained with the apparatus in Fig. 4.

of inorganic glasses and metals [10, 11]. We will use the term partly for convenience to describe the morphological features of unique periodicity and the high level of phase connectivity.

When we shine light onto a film specimen with a modulated structure, a light-scattering ring pattern is observed, as shown in Fig. 2(a). A goniometer trace of the scattered intensity gives a light-scattering profile having a peak, as shown in Fig. 2(b). The Bragg spacing from the peak corresponds to the periodic distance in the micrograph of Fig. 1(b).

We also found that a faster rate of solvent evaporation yields a shorter periodic distance in the modulated structure. Hence, one can prepare a series of film specimens with different periodic distances.

The two-phase nature in the modulated structure is confirmed by DSC studies. Figure 3 shows thermograms of BR, SBR-45, and a 50/50 blend of BR/SBR-45. In the blend specimen with modulated structure, one can see

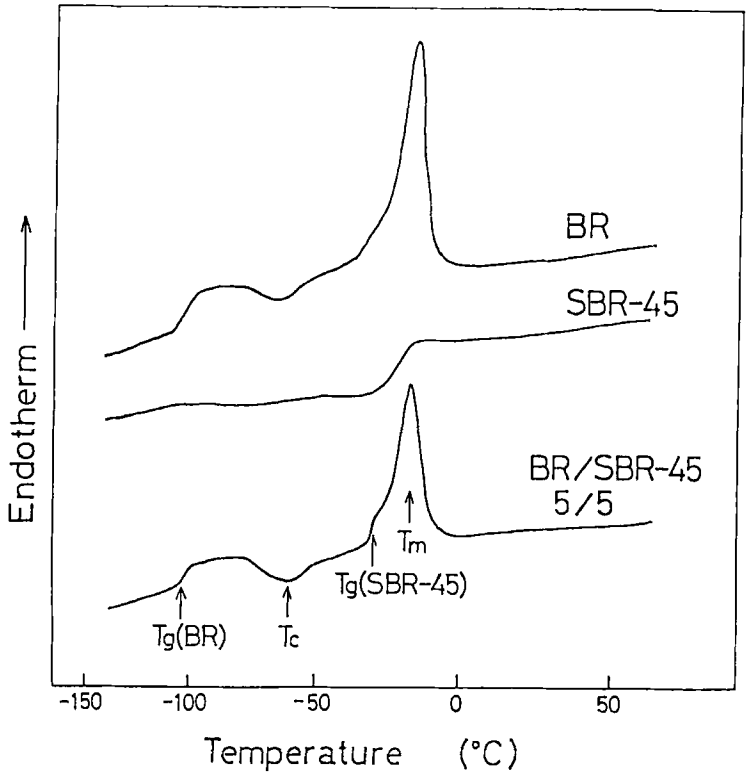

FIG. 3. DSC thermograms of BR, SBR-45, and a 50/50 blend of BR and SBR-45 with a modulated structure having a periodic distance of 2.0 μm. Scan speed: 20°C/min.

two glass transitions at the glass transition temperatures of BR and SBR-45, respectively, and also a crystallization exotherm peak and a melting endotherm peak of BR. The transition behavior suggest the two-phase nature of the modulated structure; i.e., that almost complete segregation into two pure polymer phases has taken place in the cast film.

The blend film with modulated structure is a quite novel specimen for studying a delicate change in structure with annealing, which might be overlooked in the study of a specimen with irregular structure, such as indicated in Fig. 1(a). The combination of the light-scattering technique with this novel specimen

allows quantitative discussion of the kinetics of structural change, as will be shown in the next section.

3. PHASE DIAGRAM AND KINETICS OF PHASE DISSOLUTION

In this section we describe 1) estimation of the binodal curve, 2) the kinetics of phase dissolution after a temperature jump from the two-phase region to the single-phase region, and 3) estimation of the spinodal curve by the temperature dependence of a kinetic variable. These studies were performed by employing film specimens with modulated structure and by using the light-scattering apparatus shown schematically in Fig. 4.

Figure 5 shows the results of a heating experiment with the aid of a hot stage (Linkam TH600 heating-cooling stage, Linkam Scientific Instruments, Ltd. [13]). This stage can be programmed to provide isothermal settings and also a linear temperature rise at 27 different rates between 0.1 and 90°C/min. The film specimen with modulated structure was inserted in the heating stage, and the stage was set horizontally on the light-scattering stage in Fig. 4. A He-Ne gas laser beam of 632.8 nm wavelength was applied vertically to the film specimen. A goniometer trace of the scattered light from the specimen was recorded during heating at a constant rate. As shown in Fig. 2, the light-scattering profile from the as-cast film with modulated structure has a peak.

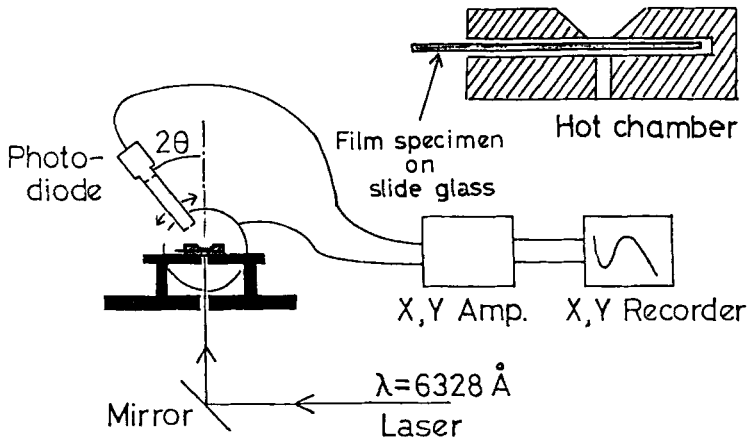

FIG. 4. Light-scattering apparatus.

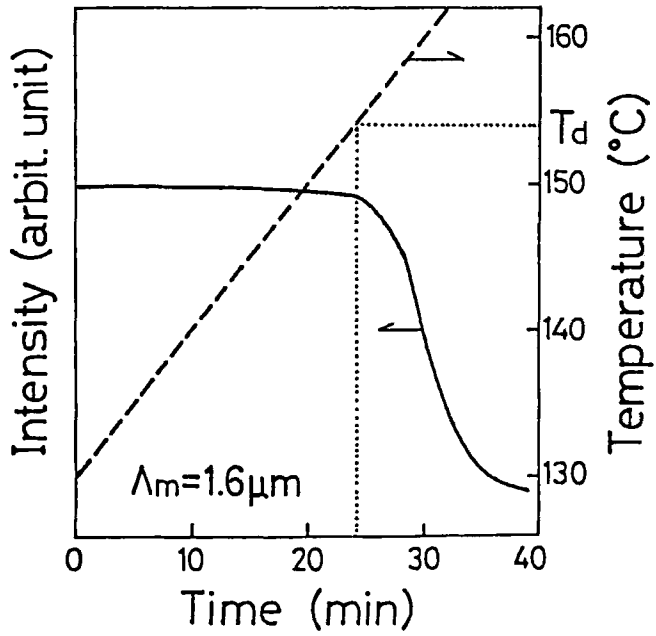

FIG. 5. Change in the peak intensity of scattered light during heating at a constant rate of 1°C/min to obtain T_d. Blend: 50/50 BR/SBR-45.

When the temperature is elevated, the light scattering profile does not change up to a certain temperature T_d. Above T_d the scattered intensity decreases with temperature, keeping the scattering peak angle constant, until the scattering peak finally disappears. T_d corresponds to the onset temperature of phase dissolution, as discussed later. T_d varied with heating rate. Selected results of T_d as a function of the heating rate are shown in Fig. 6. The intercept of T_d, at which the heating rate is zero, may correspond to the binodal temperature. Similar experiments were carried out for blend specimens of various compositions. The binodal points thus estimated are indicated by open circles in Fig. 7. An upper critical solution temperature (UCST) type phase diagram for the BR/SBR-45 system is shown in Fig. 7.

The UCST behavior was confirmed by isothermal experiments, as follows. The film specimen with the modulated structure was allowed to undergo a rapid temperature jump from room temperature to various higher temperatures set isothermally below and above the UCST. Below the USCT, no appre-

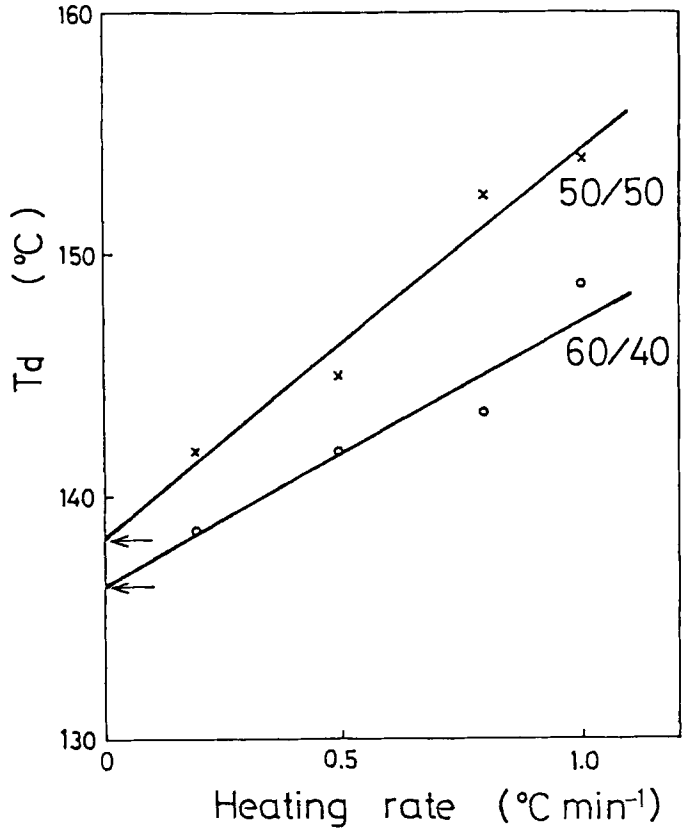

FIG. 6. T_d vs heating rate.

ciable change in the scattering profile with time of isothermal annealing could be detected on a time scale of 2 h. This means that no appreciable structural change took place. On the other hand, above the USCT, the scattered intensity decreased with time of annealing at a constant peak angle. A typical example is shown in Fig. 8. The intensity decay in Fig. 8 corresponds to the phase dissolution of the modulated structure at a constant periodic distance.

The single-phase nature after the phase dissolution is confirmed by DSC studies. Curve (a) in Fig. 9 is a DSC thermogram of the as-cast film, reproduced from Fig. 3. After the DSC run to obtain the thermogram (a), the

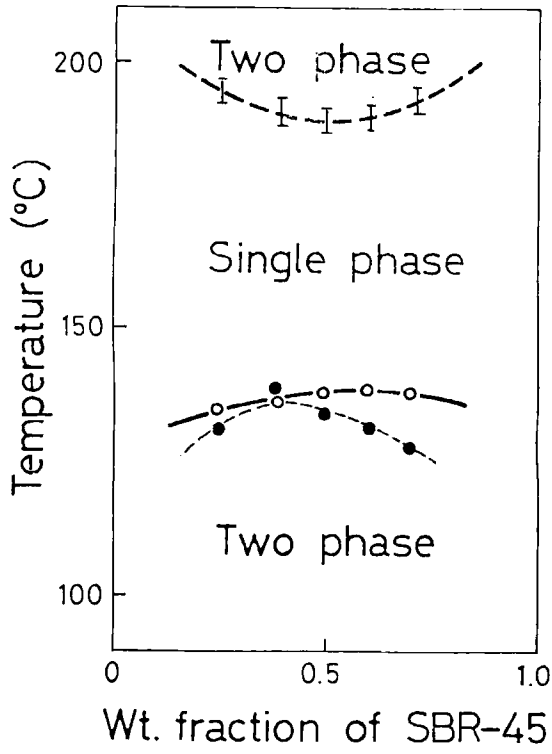

FIG. 7. Phase diagram of BR/SBR-45. (○) Binodal points estimated by extrapolation to zero heating rate. (●) Binodal points estimated by $\tilde{D}/T$ vs T plots.

film specimen was further heated to 155°C in the DSC pan and was annealed at that temperature for 30 min and then rapidly quenched to liquid nitrogen temperature. Note that the annealing condition is identical to that of the longest case in Fig. 8 at which the scattering peak has disappeared. The DSC thermogram of the annealed and quenched specimen is shown as Curve (b) in Fig. 9. All of the transitions in the as-cast film have disappeared. A broad, single glass transition is seen between the glass-transition temperatures of BR and SBR-45. This implies that the two-phase structure is transformed to an almost homogeneous solution; in other words, phase dissolution has taken place by annealing above UCST.

In Fig. 7 there is a two-phase region at higher temperatures. This LCST-

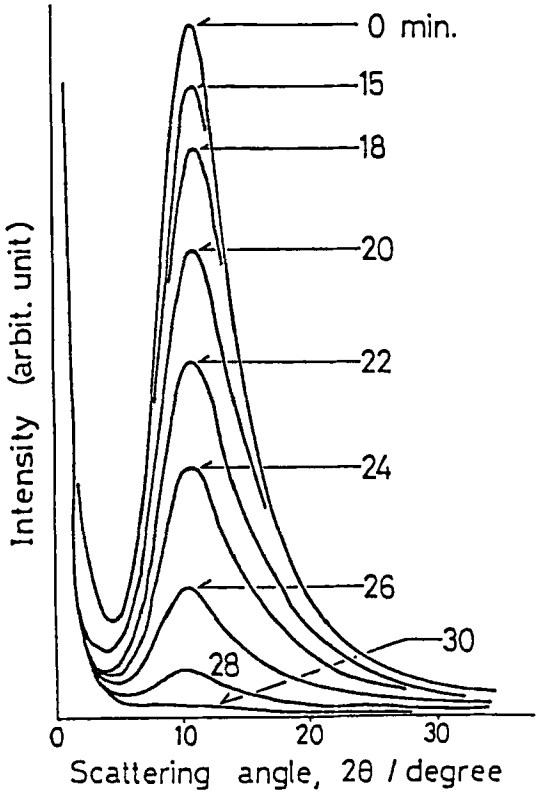

FIG. 8. Change of light-scattering profile with annealing at 155°C. Numbers are times after temperature jump. Blend: 30/70 BR/SBR-45.

type phase diagram was obtained by a dissolution and temperature jump procedure: the cast film was annealed above UCST, e.g., at 150°C for ~30 min; then the annealed specimen underwent a rapid temperature jump to an isothermal setting of higher temperatures, and the structural change was observed under the microscope and by the light-scattering technique. When no appreciable change took place, we judged that the system was still in the single-phase region. On the other hand, when the film became opaque and the scattering intensity increased, we judged that the system was in the two-phase region. On the basis of these observations, the LCST line was drawn somewhat arbitrarily in Fig. 7. Actually, we observed development of a

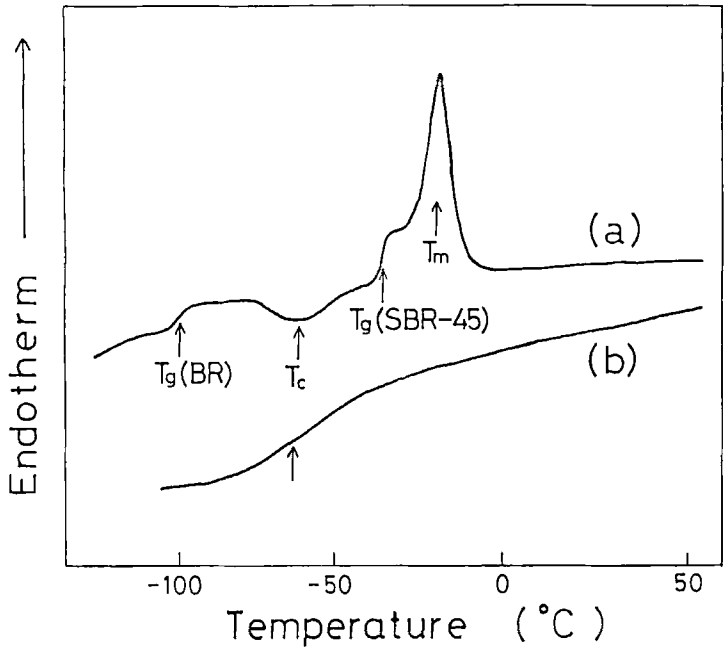

FIG. 9. DSC thermograms: (a) as-cast film, (b) film annealed at 155°C for 30 min. Blend: 50/50 BR/SBR-45.

modulated structure during isothermal annealing in the two-phase region above the LCST. It was similar in appearance to that in Fig. 1(b), but the periodic distance of the structure was much smaller than the original one in the cast film. This implies that the structural memory in the cast film had disappeared by annealing in the single-phase region, and a new concentration fluctuation had developed by spinodal decomposition induced thermally above the LCST.

Thus we see the coexistence of a UCST and a LCST in the BR/SBR-45 system [8]. This is not specific to this particular pair. Similar phase behavior has also been found in other pairs of high MW polymers such as poly(acrylonitrile-*co*-styrene)/poly(acrylonitrile-*co*-butadiene) [14], poly(methyl methacrylate)/poly(vinylidene fluoride) [15], and polystyrene/carboxylated poly(phenylene oxide) [16]. It seems to be a rather general phenomenon.

From the decay of the scattered intensity as shown in Fig. 8, we are able to discuss the kinetics of phase dissolution [17]. Figure 10 shows the change

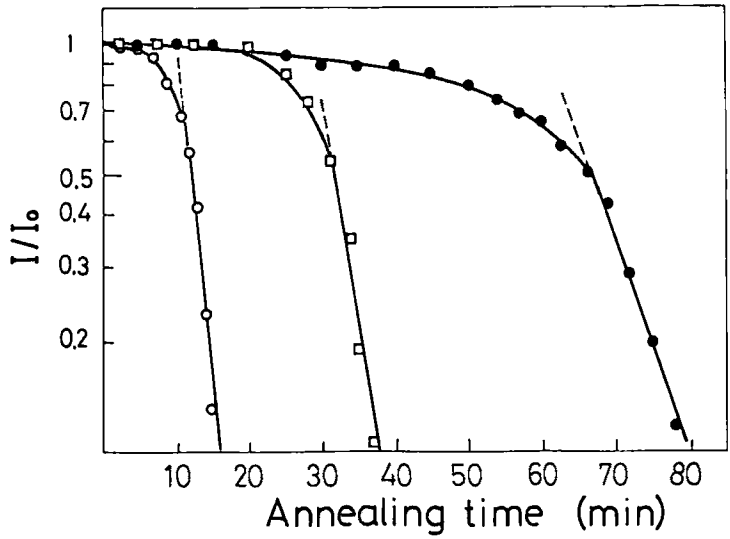

FIG. 10. Change of scattered intensity of 50/50 BR/SBE-45 blend during annealing at various temperatures: (●) 135°C (1.51 μm), (□) 145°C (1.65 μm), (○) 155°C (1.84 μm).

in peak intensity of the scattered light, I, with annealing time after the temperature jump to above the UCST. The peak intensity initially remains constant for a certain time, and then decreases exponentially with time. There seems to be a kind of induction period. The reason why an induction period exists for the phase dissolution is not obvious at present. Here we discuss the kinetics of phase dissolution from the later stage of the intensity change, i.e., by the linear decay of $\ln(I/I_0)$ vs time plots in Fig. 10, where I_0 is the peak intensity at zero annealing time. From the slope of the intensity decay, one can estimate the apparent diffusion constant $\tilde{D}$ for phase dissolution by

$$\ln(I/I_0) = -2\tilde{D}[(4\pi/\lambda)\sin(\theta_m/2)]^2 t, \quad (1)$$

where t is the time, λ is the wavelength of the light in specimen, and θ_m is the scattering peak angle [18, 19]. Similarly, we estimated the value of $\tilde{D}$ at various temperatures above the UCST, as shown in Fig. 11. The values of $\tilde{D}$ are in the range of 10^{-13}-10^{-12} cm^2/s.

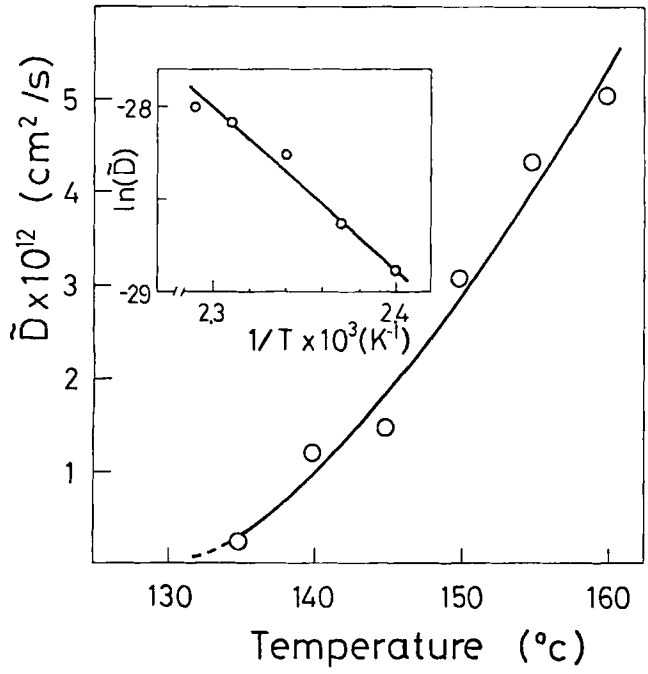

FIG. 11. Temperature dependence of apparent diffusion constant $\tilde{D}$ and its Arrhenius plot. Blends 50/50 BR/SBR-45.

By employing an Arrhenius-type expression for the apparent diffusion constant,

$$\tilde{D} = D_0 \exp(-Q/RT), \tag{2}$$

the apparent activation energy for diffusion, Q, estimated from the inset of Fig. 11, is 33.8 kcal/mol. To our knowledge, there exists only one result of Q for phase dissolution. It is 11.7 kcal/mol for the poly(vinyl chloride)/poly(ϵ-caprolactone) system according to Gilmore et al. [20]. They estimated Q by a different but more direct method: combination of scanning electron microscopy and energy-dispersive analysis of x-ray fluorescence. Our results are higher but of the same order as theirs.

We will discuss the temperature dependence of $\tilde{D}$ further. Phase dissolution is the reverse phenomenon of phase separation. However, the basic

formulation of the dynamics may be formally common for the two phenomena. The only difference is the sign of $\tilde{D}$. Thus, the theory of spinodal decomposition [9] may be applicable to the phase dissolution of the two-phase system with modulated structure. Hence, the apparent diffusion constant in dissolution is given by

$$\tilde{D} \propto D_c \left| \frac{\chi - \chi_s}{\chi_s} \right|, \tag{3}$$

where D_c is the self-diffusion coefficient for translational diffusion of polymers, χ is the Flory-Huggins interaction parameter, and χ_s is the interaction parameter at the spinodal temperature (for details, see Section 4 and Ref. 21).

Employing the relationship $D_c \propto T$ from the Stokes-Einstein equation and $|(\chi - \chi_s)/\chi_s| \propto |T - T_s|$ (T_s being the spinodal temperature), Eq. (30) leads to

$$\tilde{D} \propto T|T - T_s|. \tag{4}$$

Equation (4) implies that the $\tilde{D}/T$ versus T plot results in a straight line and that T_s can be estimated by the intercept on the T axis. Typical examples are shown in Fig. 12. The spinodal points thus estimated are indicated by the solid circles in Fig. 7. They are located reasonably; i.e., they are inside the two-phase region and depart slightly from the binodal curve. In this way we are able to estimate the spinodal curve by kinetic study of phase dissolution.

4. KINETICS OF PHASE SEPARATION IN TERNARY POLYMER MIXTURE

A large amount of knowledge has been accumulated on the kinetics of phase separation of binary polymer mixtures quenched into the two-phase region [21]. A similar kinetic study of the phase separation of ternary mixtures consisting of dissimilar polymers and solvent is significant for understanding the mechanism of phase separation during solution casting of polymer blends. This subject is related to the formation of modulated structures [22]. Figure 13 gives a framework for interpreting this situation.

In Fig. 13(a) the initial ternary solution and the casting process are indicated by the filled circle and the arrow, respectively. Now let us consider the casting process. Solvent evaporation causes the solution to enter the two-phase region in which it separates into two phases, one rich in Polymer A and the other rich in Polymer B. Phase separation in the unstable region

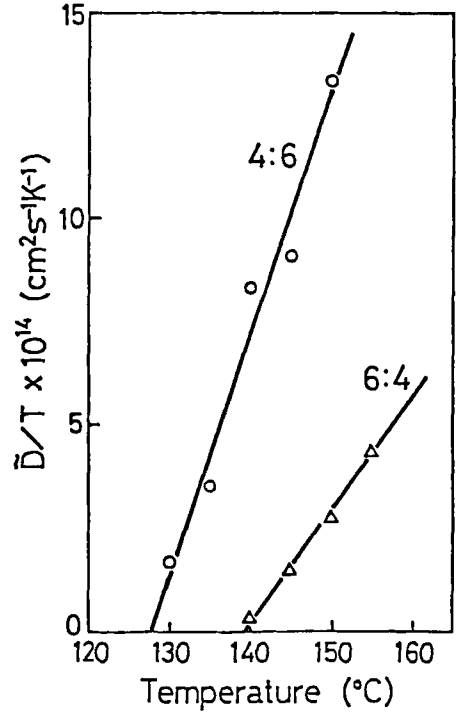

FIG. 12. $\tilde{D}/T$ vs T plots, testing Eq. (4). Spinodal temperature is obtained from the intercept on the T axis.

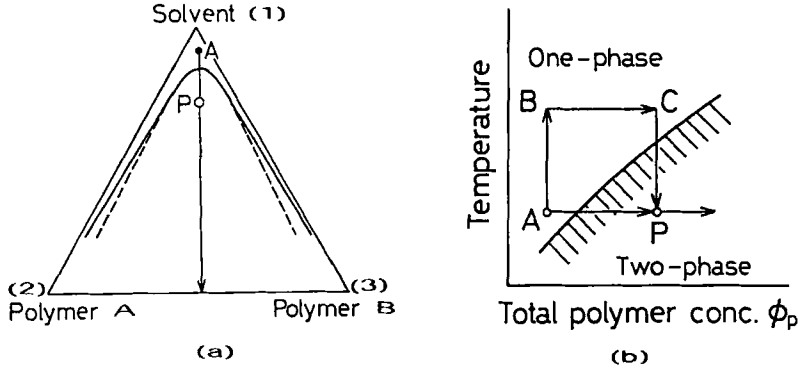

FIG. 13. (a) Phase diagram of a ternary polymer system (χ_{12} = 0.00282, χ_{13} = 0.00558, χ_{23} = 0.00872). Broken line: spinodal curve; solid line: binodal curve; arrow: casting process. (b) Temperature-drop procedure from C to P., instead of concentration jump from A to P, corresponding to the casting process.

(below the broken curve in Fig. 13a) should proceed by the spinodal decomposition mechanism. Phase separation continues during further evaporation of solvent, eventually resulting in a generally droplet-type morphology. However, if the evaporation rate is so fast that the phase-separated structure in solution has not coalesced into droplets, the phase-separated structure will be frozen in at the higher polymer concentration to result in the modulated structure of the cast film.

The above argument is based on the assumption that the prevailing mechanism of phase separation during solution casting is spinodal decomposition. To verify this assumption in a quantitative sense, we should rely on kinetic studies of phase separation in the unstable region of Fig. 13(a), e.g., at point P. However, from the experimental point of view, a concentration jump from an initial homogeneous solution to P is almost impossible. The problem may be circumvented by considering the phase diagram in Fig. 13(b). From the thermodynamic point of view, the concentration jump from A to P in Fig. 13(b) is comparable to a temperature drop from C to P. So, in order to investigate the elemental mechanism of phase separation during solution casting, kinetic studies were undertaken using a temperature-drop procedure instead of the concentration jump corresponding to the solution casting.

Figure 14 is a phase diagram of a ternary system studies (BR/SBR-45/toluene). The solid line is the cloud-point curve dividing the homogeneous region and the two-phase region. The temperature-drop experiments were carried out in a light-scattering photometer (Shimazu, Model PG-21), which is commonly used for studies of dilute polymer solutions. On placing the ternary solution, sealed in a NMR tube with diameter of 6.7 mm, in a silicone oil bath in the light-scattering apparatus, the solution underwent a rapid temperature drop to new isothermal conditions. The change of the angular distribution of scattered light intensity with time was measured during the isothermal phase-separation process.

Figure 15 is a typical example of the change of scattered intensity with time at various values of q. The parameter q is the magnitude of the scattering vector given $q = (4\pi/\lambda) \sin(\theta/2)$, where λ is the wavelength in the solution and θ is the external scattering angle. In the initial stages of phase separation, the scattered intensity increases exponentially with time. In the later stage, the intensity increase deviates from the exponential curve.

According to Cahn's linear theory of spinodal decomposition [9], the exponential increase of the scattered intensity is described by

$$I(q,t) \propto \exp[2R(q)t], \tag{5}$$

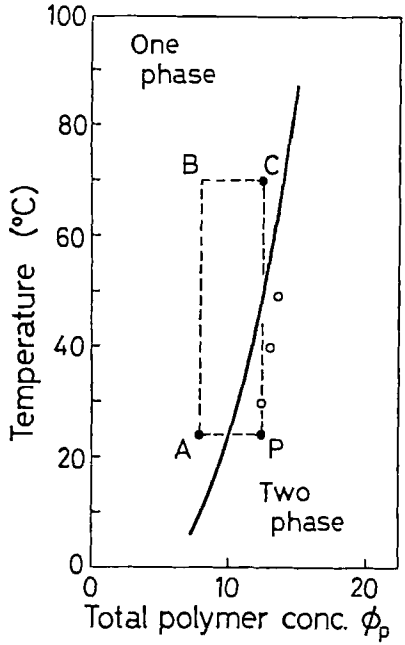

FIG. 14. Phase diagram of BR/SBR-45/toluene system (50/50 BR/SBR-45) and a temperature-drop procedure from C to P. The solid line is the cloud-point curve. The open circles are spinodal points obtained from the kinetic studies in Figs. 15-17.

where I is the scattered intensity, t is the time after the initiation of spinodal decomposition, and $R(q)$ is the growth rate of concentration fluctuation having wavenumber q. $R(q)$ is given by

$$R(q) = -Mq^2\left(\frac{\partial^2 f}{\partial c^2} + 2\kappa q^2\right), \tag{6}$$

where M is the mobility, κ is the gradient energy coefficient, f is the free energy of the solution, and c is the concentration. According to Eq. (5), a plot of $\ln I$ versus t at a fixed q should yield a straight line of slope $2R(q)$. A linear relationship is obtained for the initial stage of phase separation, as shown in Fig. 15, indicating that it can be described by the linearized spinodal decomposition theory. Linear results are also obtained for solutions with other concentrations at various temperatures.

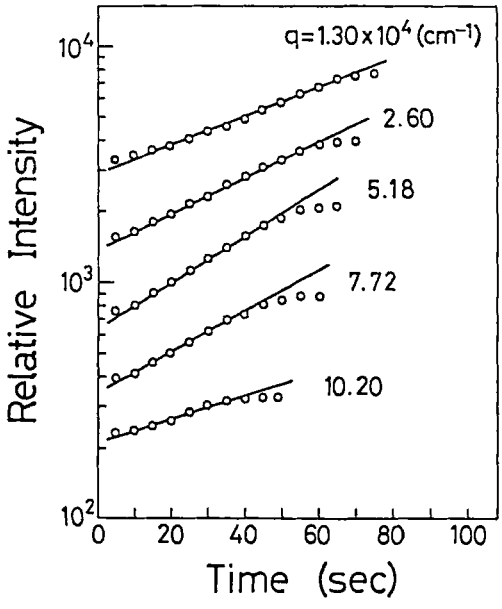

FIG. 15. Change of scattered light intensity at various values of q for a BR/SBR-45/toluene solution quenched to and then kept at 20°C, demonstrating the exponential character of $I(t)$ at the initial stage of phase separation.

In Fig. 16, $R(q)/q^2$ is plotted versus q^2. In agreement with Eq. (4), the data yield a straight line, indicating again that at least the initial stage can be described within the framework of the linear theory. From the plots, one can obtain the characteristic parameters, such as q_m, q_c, and $\tilde{D}$, describing the dynamics of phase separation, where q_c is the critical (maximum) wavenumber of fluctuation which can grow and q_m is the most probable wavenumber of fluctuation having the highest rate of growth. According to Eq. (6), q_c is given by the intercept on the q^2 axis, while q_m is calculated by $q_m{}^2 = (1/2)q_c{}^2$ The apparent diffusion coefficient $\tilde{D}$, defined by $-M(\partial^2 f/\partial c^2)$, is given by the intercept on the vertical axis.

Figure 17 shows the temperature dependence of $\tilde{D}$. The intercept of T, at $\tilde{D} = 0$, gives an estimate of the spinodal temperature T_s at which $(\partial^2 f/\partial c^2) = 0$, hence $\tilde{D}$ is zero. The spinodal points thus estimated are indicated by open circles in Fig. 14. These seem to be reasonable, i.e., they are inside the two-phase region and slightly apart from the binodal curve.

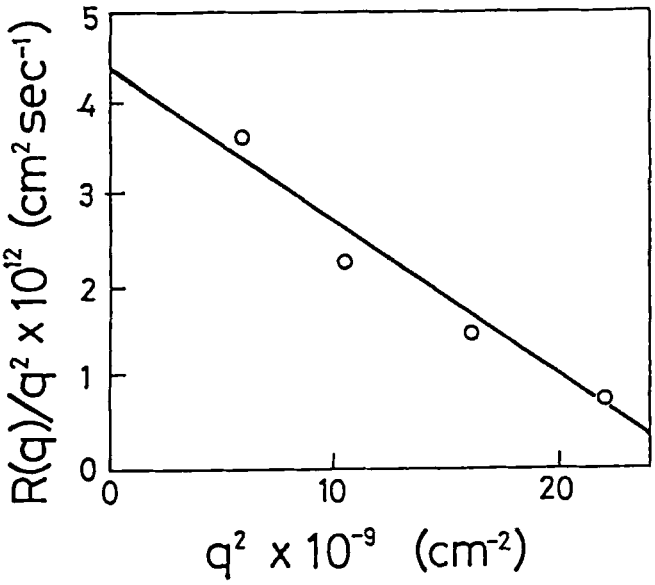

FIG. 16. Plots of $R(q)/q^2$ vs q^2, testing Eq. (4).

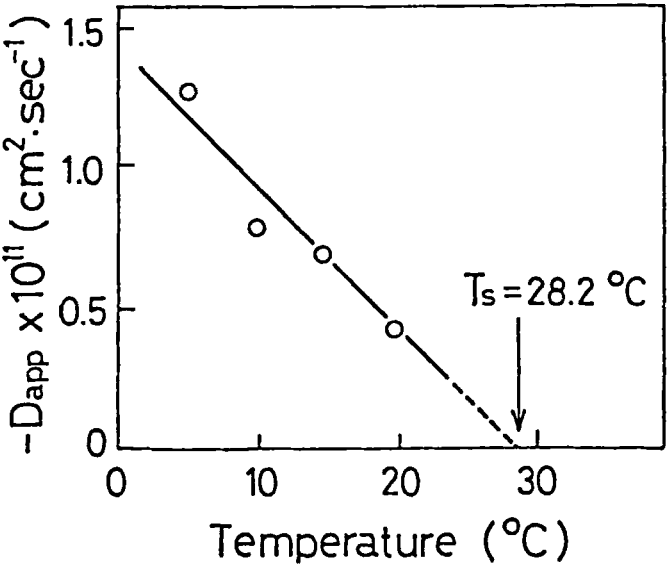

FIG. 17. Temperature dependence of apparent diffusion constant $\tilde{D}$.

Further, during the later stage of phase separation, we observed a light-scattering ring pattern similar to Fig. 2(a). The peak angle of the ring pattern was slightly smaller than that expected from the q_m of the initial stage. All these results suggest that the elemental mechanism of phase separation is spinodal decomposition.

5. LIGHT SCATTERING IN THE SINGLE-PHASE REGIME AND PHASE BEHAVIOR

So far, we have mostly discussed the light scattering from the phase-separated systems. In this section we deal with the scattering from single-phase polymer systems. A ternary mixture of dissimilar polymers and solvent, such as in the previous section, scatters light even in the single-phase region. The scattered intensity is very weak in comparison to that from two-phase polymer systems but is fairly strong in comparison to that from dilute polymer solutions. The analysis of light scattering in the single-phase region is based on the de Gennes' scattering function $S(q)$ [23]. For the ternary polymer mixture, however, we need a modified version of the $S(q)$ method [24]. Hence, we first describe the theoretical background very briefly.

De Gennes derived a scattering function $S(q)$ for homogeneous binary polymer blends by the random phase approximation:

$$S^{-1}(q) = [N_A \phi g_D(R_{gA}{}^2 q^2)]^{-1} + [N_B(1-\phi) g_D(R_{gB}{}^2 q^2)]^{-1} - 2\chi, \tag{7}$$

where N is the number of segments per polymer chain, ϕ is the volume fraction of Polymer A, R_g is the radius of gyration of the chain, and g_D is the Debye function for a Gaussian chain:

$$g_D(x) = 2x^2(x - 1 + e^{-x}). \tag{8}$$

In the low q regime ($R_g q \ll 1$), the Debye function is approximated by

$$g_D(x) \doteqdot 1 - \frac{x}{3} = 1 - (1/3) R_g{}^2 q^2. \tag{9}$$

Hence, in the case of $R_g = R_{gA} = R_{gB}$, $S(q)$ is given by

$$S^{-1}(q) = 2(\chi_s - \chi) + \frac{2\chi_s}{3} R_g{}^2 q^2, \tag{10}$$

where χ_S is the interaction parameter at the spinodal point. It is convenient to rewrite this equation in the standard form

$$\frac{S(q)}{S(0)} = \frac{1}{1 + \xi^2 q^2}, \tag{11}$$

where ξ is the correlation length defined by

$$\xi^2 = \frac{R_g^2}{3} \left| \frac{\chi_S}{\chi_S - \chi} \right|. \tag{12}$$

Equation (11) expresses the Ornstein-Zernike form [25] for small q. By employing this $S(q)$ formulation. Shibayama et al. [26] estimated ξ, χ, and the phase diagram in a mixture of deuterated polystyrene and hydrogenated poly(vinyl methyl ether) by small-angle neutron scattering (SANS). Bates et al. [27, 28] also applied this $S(q)$ method to SANS studies for a binary mixture of protonated and deuterated 1,4-polybutadiene.

In the high q regime ($R_g q \gg 1$), on the other hand, Eq. (8) is approximated by

$$g_D(\chi) \doteqdot \frac{2}{R_g^2 q^2}, \tag{13}$$

and the last term of Eq. (7) is negligible. Hence,

$$S(q) = \frac{2N\phi(1 - \phi)}{R_g^2 q^2}. \tag{14}$$

Equation (14) involves no thermodynamic parameter related to the phase behavior. Therefore, scattering studies in the large q regime do not fit out objective.

In our ternary polymer solution, the component polymers have many thousands of segments whose length may be ~ 0.5-1.0 nm, and the polymers are dissolved in a good solvent. The light in our scattering study is from a He-Ne laser (λ = 632.8 nm). The angular distribution of scattered light is measured over a range of scattering angle θ from 20 to 120°. For this experimental situation, the scattering function of Eq. (10) approximated for the small q regime is not appropriate. A scattering function derived for the intermediate q regime ($R_g q \approx 1$) should be applied for our experiments.

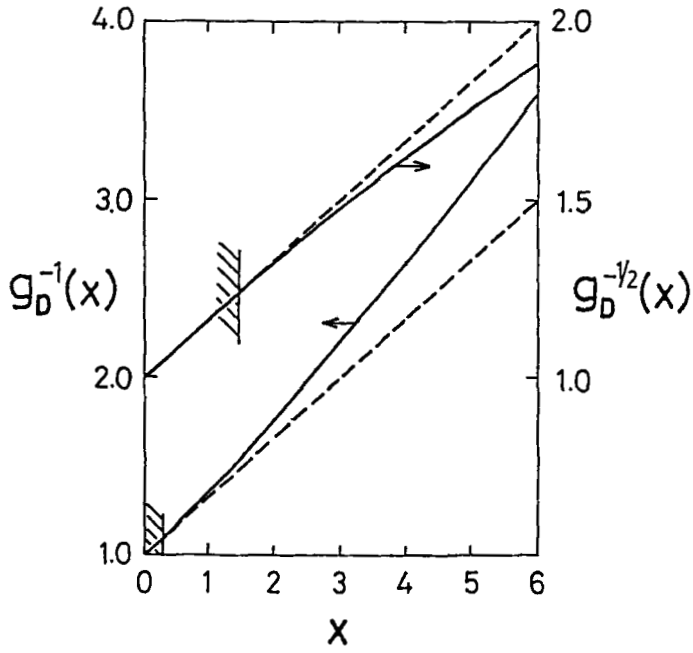

FIG. 18. Relationship between Debye function $g_D(x)$ and its approximate equation. The solid lines and the broken lines represent the Debye function (Eq. 8) and its approximate equations (Eqs. 9 and 15). The range of x where the function $g_D^{-1/2}(x)$ and $g_D^{-1}(x)$ deviate from the respective broken lines by less than 2% are shown by the shaded lines [29, 30].

Truncating the series expansion of Eq. (8) at the third term, we have

$$g_D^{-1}(x) = 1 + \frac{1}{3}x + \frac{1}{36}x^2. \tag{15}$$

This is a good approximation in the $R_g q \approx 1$ regime, as shown in Fig. 18. Inserting Eq. (15) into Eq. (7), we have

$$S^{-1}(q) \doteq \frac{1}{2(\chi_s - \chi)} \left\{ 2(\chi_s - \chi) + \frac{2\chi_s}{6} R_g^2 q^2 \right\}^2. \tag{16}$$

It is convenient to rewrite this equation in the standard form

$$\frac{S(q)}{S(0)} = \frac{1}{(1+\xi^2 q^2)^2}, \tag{17}$$

where

$$\xi^2 = \frac{R_g^2}{6}\left|\frac{\chi_s}{\chi_s - \chi}\right| \propto \left|\frac{T - T_s}{T_s}\right|^{-1}. \tag{18}$$

Equation (17) is just the Debye-Bueche form [31].

It is interesting that the scattering function is expressed by two familiar forms in different regimes, i.e., the Ornstein-Zernike form in the regime of $R_g q \ll 1$ and the Debye-Bueche form in the regime of $R_g q \sim 1$.

The experimental procedure for the $S(q)$ method is the same as that for dilute polymer solutions. We used the same specimens and the same light-scattering apparatus as in the previous section.

Figure 19 shows typical examples of the Debye-Bueche plot. $I^{1/2}$ versus q^2. As expected from Eq. (17), the plots are good straight lines at various concentrations. Similar results are obtained at different temperatures.

From the linear plots in Fig. 19, one can estimate the values of the correlation length ξ. The ξ values obtained are plotted in Fig. 20 as a function of measured temperature T for a fixed concentration. As expected from Eq. (18), ξ^{-2} is proportional to $|T - T_s|$. The spinodal temperature T_s is given by the intercept on the T axis.

Figure 21 shows plots of ξ^{-2} versus the total polymer concentration ϕ_p. Following the dilute approximation by Scott (32), the Flory-Huggins interaction parameter χ in ternary solution (Polymer A/Polymer B/solvent) is given by $\chi = \chi_{AB}\phi_p$. This implies that the solvent simply acts as a diluent to decrease χ_{AB}, the interaction parameter between Polymers A and B. Hence, from Eq. (18),

$$\xi^{-2} \propto \left|\frac{\chi - \chi_s}{\chi_s}\right| \propto \left|\frac{\phi_p - \phi_{p,c}}{\phi_{p,c}}\right|, \tag{19}$$

where $\phi_{p,c}$ is the total polymer concentration at the spinodal point. As expected from Eq. (19), the plot of ξ^{-2} versus ϕ_p in Fig. 21 is a good straight line. From the intercept on the ϕ_p axis, one can obtain the value of $\phi_{p,c}$ at which $\xi^{-2} = 0$ or $\xi = \infty$. Figure 21 also includes the ξ data obtained in the

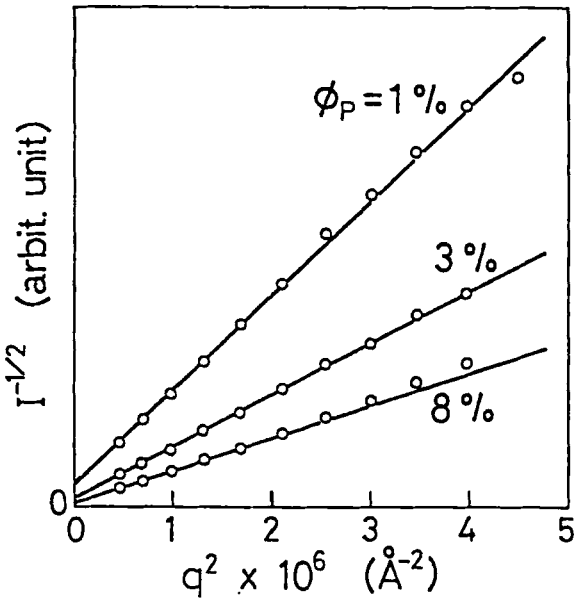

FIG. 19. Debye-Bueche plots for BR/SBR-45/toluene solutions for various polymer concentrations at 25°C.

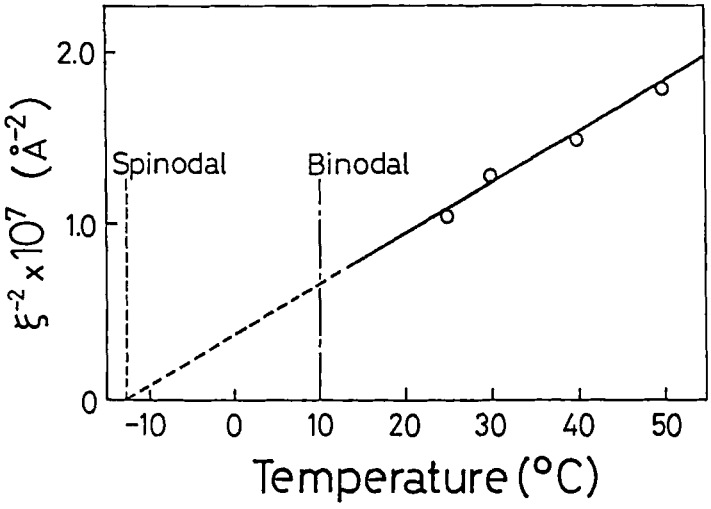

FIG. 20. Inverse square of correlation length vs temperature. ϕ_p = 8 wt%.

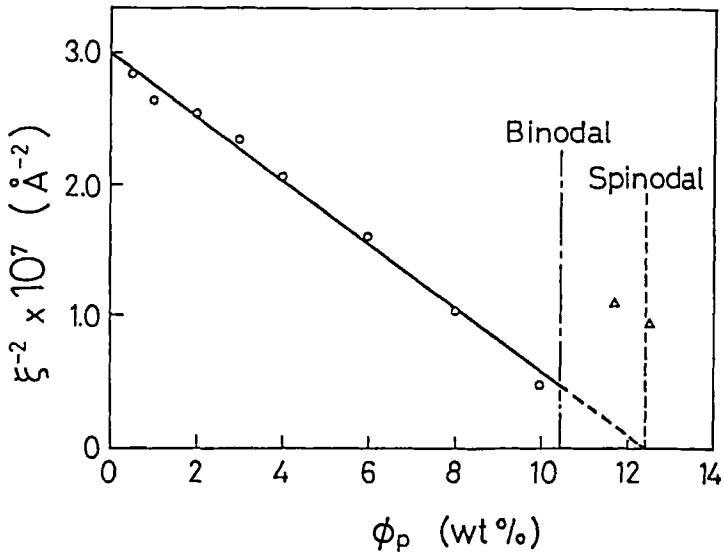

FIG. 21. Inverse square of correlation length vs total polymer concentration plots at 25°C.

metastable region (between the binodal and the spinodal curves). These are indicated by triangles and deviate from the straight line. This is a natural result because phase separation had already taken place in the solution in the metastable state before the scattering measurement.

The spinodal points thus estimated by extrapolating along the T axis and also the ϕ_p axis are indicated by the triangles in Fig. 22. In this figure the spinodal curve from the kinetic measurements is shown as the broken line taken from Fig. 14. The triangles are located right on the broken line. It implies that the agreement between the kinetic results and the static ones by the $S(q)$ method is quite good, confirming the validity of the static analysis based on the Debye-Bueche scattering function.

It is interesting that the behavior of the correlation length in the single-phase region did not depend on the way the critical point is approached; i.e., through the temperature change or through the concentration change, the critical behavior can be described in terms of the same exponent.

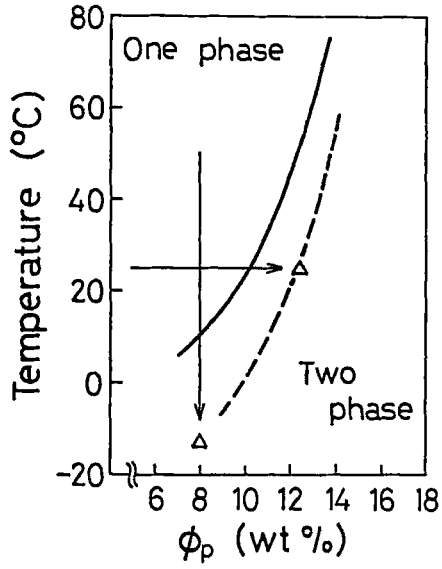

FIG. 22. Phase diagram of the BR/SBR-45/toluene system (50/50 BR/SBR-45). The solid and broken lines represent the cloud point and the spinodal curves, respectively, obtained by kinetic studies. The triangles show the spinodal points from the static studies.

REFERENCES

[1] D. R. Paul and S. Newman (eds.), *Polymer Blends,* Academic, New York, 1978.

[2] S. Akiyama, T. Inoue, and T. Nishi, *Polymer Blends–Compatibility and Interface,* CMC Press, Tokyo, 1979.

[3] O. Olabishi, L. M. Robeson, and M. T. Shaw, *Polymer-Polymer Miscibility,* Academic, New York, 1979.

[4] T. Inoue, T. Ouguzawa, O. Yasuda, and K. Miyasaka, *Macromolecules, 18,* 57 (1985).

[5] H. Kawatoh, M. Kakimoto, A. Tanioka, and T. Inoue, *Ibid., 21,* 625 (1988).

[6] K. Sato (Nishiboseki Co., Ltd.), Private Communication.

[7] T. Ougizawa and T. Inoue, *J. Mater. Sci., 23,* 718 (1988).

[8] T. Ougizawa, T. Inoue, and H. W. Kammer, *Macromolecules, 18,* 2089 (1985).

[9] J. W. Cahn, *J. Chem. Phys., 42,* 93 (1965).
[10] W. J. Cahn, *Trans. Metall. Soc. AIME, 242,* 166 (1968).
[11] H. Hilliard, M. Cohen, and B. L. Averbach, *Acta Metall., 9,* 536 (1961).
[12] R. S. Stein and M. B. Rhodes, *J. Appl. Phys., 31,* 1873 (1970).
[13] T. Shephered, *Econ. Geol., 76,* 1244 (1981).
[14] T. Ougizawa and T. Inoue, *Polym. J., 18,* 521 (1986).
[15] H. Saito, Y. Fujita, and T. Inoue, *Ibid., 19,* 405 (1987).
[16] G. Cong, Y. Haung, W. J. MacKnight, and F. E. Karasz, *Macromolecules, 19,* 2765 (1986).
[17] T. Takagi, T. Ougizawa, and T. Inoue, *Polymer, 28,* 103 (1987).
[18] H. Eichler, G. Salje, and H. J. Stahl, *J. Appl. Phys., 44,* 5383 (1973).
[19] T. Hashimoto, T. Tsukahara, and H. Kawai, *Macromolecules, 14,* 708 (1981).
[20] P. T. Gilmore, R. Falabella, and R. L. Laurence, *Ibid., 13,* 880 (1980).
[21] T. Hashimoto, M. Itakura, and H. Hasegawa, *J. Chem. Phys., 85,* 6118 (1986); and references cited therein.
[22] T. Inoue, T. Ougizawa, and K. Miyasaka, in *Current Topics in Polymer Science* (R. M. Ottenbrite, L. A. Utracki, and S. Inoue, eds.), Hanser, New York, 1987, p. 244.
[23] P.-G. de Gennes, *Scaling Concept in Polymer Physics,* Cornell University Press, Ithaca, New York, 1979.
[24] T. Ougizawa and T. Inoue, *Macromolecules,* Submitted.
[25] L. S. Ornstein and F. Zernike, *Proc. Acad. Sci., 17,* 193 (1914).
[26] M. Shibayama, H. Yang, R. S. Stein, and C. C. Han, *Macromolecules, 18,* 2179 (1985).
[27] F. S. Bates, G. D. Wignall, and W. C. Koehler, *Phys. Rev. Lett., 55,* 2425 (1985).
[28] F. S. Bates, S. B. Dierker, and G. D. Wignall, *Macromolecules, 19,* 1938 (1986).
[29] G. C. Berry, *J. Chem. Phys., 44,* 4550 (1966).
[30] H. Uchiyama, Y. Tsunashima, and M. Kurata, *Ibid., 55,* 3133 (1971).
[31] P. Debye and A. M. Bueche, *J. Appl. Phys., 20,* 518 (1949).
[32] R. L. Scott, *J. Chem. Phys., 17,* 279 (1949).